

Near-infrared *H*- and *K*-band studies of the 2006 outburst of the recurrent nova RS Ophiuchi

D. P. K. Banerjee,[★] R. K. Das[★] and N. M. Ashok[★]

Physical Research Laboratory, Navrangpura, Ahmedabad 380009, India

Accepted 2009 June 18. Received 2009 June 2; in original form 2008 December 31

ABSTRACT

We present near-infrared photospectroscopy in the *H* and *K* bands of the 2006 outburst of the recurrent nova RS Ophiuchi. The observations cover the period between 1 and 94 d after the eruption. The near-infrared light curve is presented. An extensive set of spectra is presented, lines identified and the general characteristics of the spectra discussed. Analysis of the H α line profiles shows the presence of broad wings on both flanks of a strong central component indicating the presence of a bipolar velocity flow in the ejecta. Such a flow is kinematically consistent with the bipolar structure that the object displays in high-resolution spatial images. We discuss the behaviour and origin of the Fe II lines at 1.6872 and 1.7414 μm that are prominently seen throughout the span of the observations. It is examined and shown that Lyman α and Lyman continuum fluorescence are viable mechanisms to excite these lines. We draw upon the result, that collisional excitation can also contribute in exciting and significantly enhancing the strength of these Fe II lines, to propose that these lines originate from a site of high particle density. Such a likely site could be the high-density, low-temperature contact surface that should exist in the shock front in between the shocked ejecta and red giant wind. Recombination analysis of the H α lines indicates deviations from case B conditions during most of the span of our observations indicating optical depth effects. It appears likely that the breakout of the shock front had not yet occurred till the end of our observations. An analysis is made of the temporal evolution of the [Si VI] 1.9641 μm coronal line and another coronal line at 2.0894 μm which is attributed to [Mn XIV]. Assuming collisional effects to dominate in the hot coronal gas, estimates are made of the ion temperature in the gas.

Key words: line: identification – techniques: photometric – techniques: spectroscopic – stars: individual: RS Ophiuchi – novae, cataclysmic variables.

1 INTRODUCTION

The recurrent nova RS Ophiuchi (RS Oph) underwent its most recent outburst on 2006 February 12.83. It was discovered at $V = 4.5$ near the optical peak (Hirosawa 2006). The earlier outbursts of RS Oph have been well documented – the previous eruptions having occurred in 1898, 1933, 1958 and 1985. The RS Oph binary system composed of a white dwarf (WD) primary accompanied by a red giant secondary – the orbital period of the system being 455.72 ± 0.83 d (Fekel et al. 2000). A more recent study by Brandi et al. (2009) finds a closely similar value of 453.6 ± 0.4 d for the orbital period. There is some uncertainty regarding the exact classification of the secondary companion – suggested classifications range from K0 III to M4 III with M2 III being the most likely (Worters et al.

2007 and references therein). The recent outburst has been studied in great details at several wavelength regimes viz. in X-rays (e.g. Bode et al. 2006; Sokoloski et al. 2006), in the optical (Buil 2006; Fujii 2006; Iijima 2006; Skopal et al. 2009), in the infrared (IR; e.g. Das, Banerjee & Ashok 2006; Monnier et al. 2006; Evans et al. 2007a) and in the radio (e.g. O’Brien et al. 2006; Kantharia et al. 2007; Rupen, Mioduszewski & Sokoloski 2008). In our previous study (Das et al. 2006), we had presented and analysed the *J*-band near-IR data. Our focus, at that stage, was on the IR detection and behaviour of a shock wave that is generated as the high-velocity ejecta from the outburst interacts with the pre-existing red giant wind. The velocity changes in the propagating shock front, notably its rapid deceleration, were inferred by noting the large changes in the linewidths of the Paschen β (Pa β) 1.2818 μm and the Ly β fluoresced OI 1.1287 μm lines in the *J* band. In the present work, we study the general near-IR characteristics of the present eruption in greater detail. To achieve this, we extend the analysis of some of the earlier *J*-band data but, more importantly, present new and

[★]E-mail: orion@prl.res.in (DPKB); rkdas@prl.res.in (RKD); ashok@prl.res.in (NMA)

extensive *H* and *K* spectroscopic and photometric observations of RS Oph up to 94 d after its outburst.

2 OBSERVATIONS

RS Oph was observed regularly since its discovery on 2006 February 12.83. Both spectroscopic and photometric observations in the near-IR *JHK* bands were obtained at the Mt. Abu 1.2-m telescope. The spectra were obtained at similar dispersions of $\sim 9.75 \text{ \AA pixel}^{-1}$ in each of the *J*, *H*, *K* bands using the Near Infrared Imager/Spectrometer with a 256×256 HgCdTe Near Infrared Camera and Multi-Object Spectrometer 3 (NICMOS3) array. The log of spectroscopic observations has been presented in Table 1. In each of the bands, generally a set of at least two spectra was taken with the nova off-set to two different positions along the slit (slit width ~ 1 arcsec). The dithered spectra were subtracted from each other to remove the contribution from the sky. In order to remove telluric features in the object spectra, spectra of a standard star (SAO 122754; spectral type A0V) were also recorded; the general attempt always being to obtain the object and standard star spectrum at the same airmass. The spectra were extracted and analysed using the APEXTRACT task in IRAF, and wavelength calibration was done using a combination of OH sky lines and telluric lines that register with

Table 1. A log of the spectroscopic observations of RS Oph. The date of outburst is taken to be 2006 February 12.83 UT.

Date 2006 (UT)	Days since outburst	Integration time		
		<i>J</i>	<i>H</i>	<i>K</i>
February 13.9929	1.1629	10	10	10
February 14.9915	2.1615	10	10	10
February 15.9898	3.1598	10	10	10
February 16.9866	4.1566	10	10	10
February 19.9759	7.1459	10	8	10
February 20.9721	8.1421	5	8	10
February 21.9463	9.1163	10	10	15
February 22.9505	10.1205	10	10	10
February 24.9705	12.1405	10	10	10
February 26.9926	14.1626	10	10	10
February 28.9542	16.1242	15	10	10
March 02.9465	18.1165	20	20	20
March 16.9465	32.1165	20	30	30
March 17.8866	33.0566	30	30	30
March 18.9372	34.1072	30	30	30
March 19.8833	35.0533	30	30	30
March 20.8733	36.0433	45	30	30
March 22.8682	38.0382	45	45	45
March 26.8778	42.0478	60	60	60
March 27.8644	43.0344	60	60	60
March 29.8462	45.0162	75	90	90
March 30.8629	46.0329	75	90	90
March 31.8701	47.0401	90	90	90
April 02.8736	49.0436	90	120	120
April 03.9691	50.1391	90	120	120
April 05.9607	52.1307	90	90	90
April 10.8936	57.0636	90	120	90
April 12.8454	59.0154	90	120	90
April 22.9392	69.1092	90	90	90
April 29.8355	76.0055	120	120	120
May 01.8149	77.9849	120	180	180
May 03.810	79.980	180	180	180
May 11.8353	88.0053	270	270	270
May 17.8103	93.9803	270	270	270

Table 2. A log of the photometric observations of RS Oph. The date of outburst is taken to be 2006 February 12.83 UT.

Date 2006 (UT)	Days since outburst	Magnitudes		
		<i>J</i>	<i>H</i>	<i>K</i>
February 23.9518	11.1218	4.82	4.54	3.85
February 27.9259	15.0959	5.12	4.79	4.19
March 01.9485	17.1185	5.30	4.97	4.42
March 21.8986	37.0686	6.46	6.12	5.64
March 22.9645	38.1545	6.43	6.14	5.63
March 26.9534	42.1234	6.67	6.23	5.75
March 27.9189	43.0889	6.69	6.30	5.81
March 29.9696	45.1396	6.73	6.32	5.81
April 29.9037	76.0737	7.12	6.53	6.33
May 01.8913	78.0613	7.16	6.56	6.43
May 03.8845	80.0545	7.35	6.55	6.49
May 11.9199	88.0899	7.57	6.92	6.56
May 17.9127	94.0827	7.86	7.01	6.74

the stellar spectra. Following the standard reduction procedure, the hydrogen Pa and Brackett (Br) absorption lines were first removed by manual extrapolation from the spectra of the comparison star. While the absorption lines are generally well removed in this process, it is estimated that residuals amounting to 5 per cent of the line strength may still remain. The nova spectra were then divided by the spectrum of the comparison star; these ratioed spectra were multiplied by a blackbody curve corresponding to the effective temperature of the comparison star to yield the final spectra. The ratioing process, while removing telluric features sufficiently well, leaves some residuals in the wavelength regions where telluric absorption is strong. This applies significantly to the region around $2.0 \mu\text{m}$ in the *K* band which is strongly affected by atmospheric carbon dioxide.

The *JHK* photometry of RS Oph was done under photometric sky conditions using the imaging mode of the NICMOS3 array. In each of the *J*, *H*, *K* filters, several frames in five dithered positions, offset typically by ~ 20 arcsec, were obtained of both the nova and a selected standard star. Photometric reduction was done using the aperture photometry task APPHOT in IRAF. The derived *JHK* magnitudes, with typical errors in the range of 0.01 to 0.03 mag, along with the log of the photometric observations are given in Table 2.

3 RESULTS

3.1 Photometry: the *JHK* light curve

We present in Fig. 1 the *JHK* light curves of RS Oph using photometric data obtained between 11 and 94 d after outburst. Although we would have liked to have sampled the light curve more frequently, our efforts were focused more on the spectroscopy. Furthermore, superimposed in Fig. 1 is the near-IR light curve of the 1985 outburst which was obtained by Evans et al. (1988). While it is known that the visual light curve behaves similarly from outburst to outburst (Rosino & Iijima 1987), an equivalent comparison for the near-IR light curve had not been possible earlier for lack of data. The present data show that the IR decline is quite similar to that of the 1985 outburst. However, some caution is needed while comparing the near-IR light curves because of the effect of emission lines on the measured continuum flux in the photometric bands. The *JHK* spectra of RS Oph has prominent emission lines, some of which lie at the edge of the photometric bands. Filter transmissions

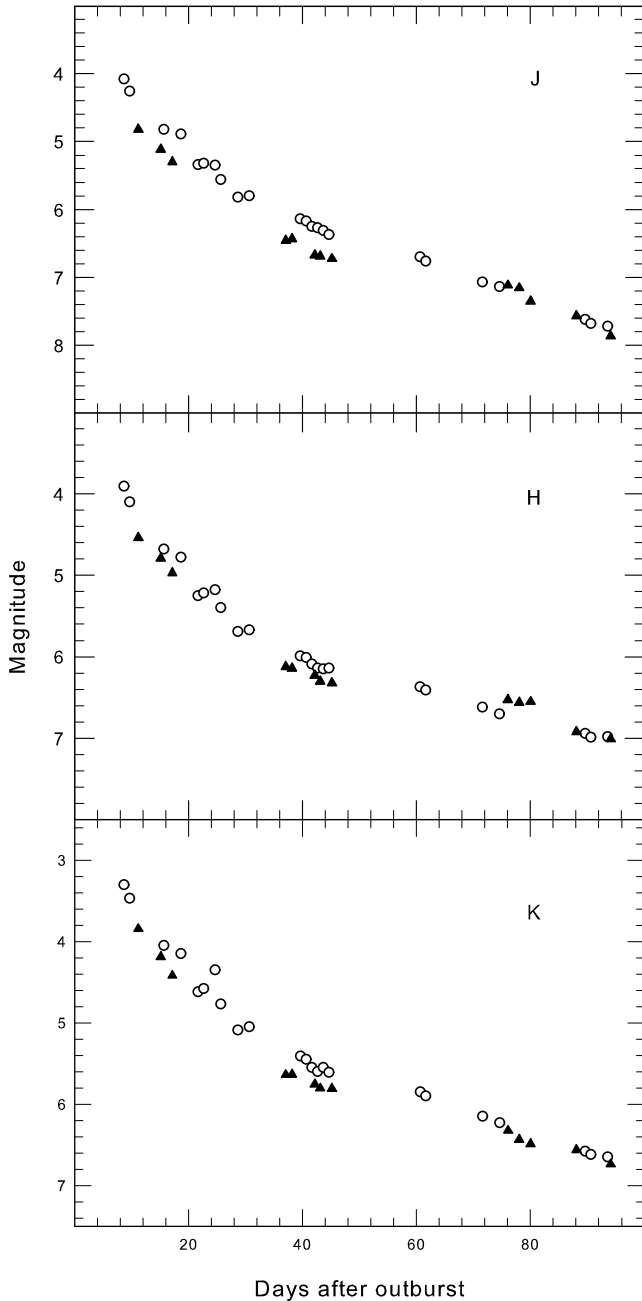


Figure 1. The *J*, *H*, *K* light curves for RS Oph, based on data from Table 2, are shown with filled triangles. To show the similarity of the light curve behaviour from different outbursts, the data from the 1985 outburst (Evans et al. 1988) are also shown with open circles.

in these regions can vary significantly in different photometric systems thereby contributing different amounts of the line flux to the measured continuum. For example, Whitelock et al. (1984) point out the significant effect of the He I 1.083 μm line on the measured *J* magnitudes in emission line stars (the He I line lies at the edge of the *J* band and can be strong).

A compilation of several observations of the pre-outburst or quiescent photometry of RS Oph shows that it has a mean pre-outburst values of $J = 7.72$, $H = 6.945$, $K = 6.66$ (Evans et al. 1988; table 1 therein). From our data we see that in each of the *JHK* bands the magnitude returned to its pre-outburst value by ~ 88 d. Our last

observation on day 94 suggests that the decline appears to continue below this level – such a trend was clearly seen by Evans et al. (1988) for the 1985 outburst.

3.2 Spectroscopy: general characteristics of the *JHK* spectra and line identification

Although spectra of RS Oph were obtained on several days, we present in Figs 2 and 3 selected *H*- and *K*-band spectra that suffice to give the general trend of the spectral evolution of the object. Since a similar mosaic for the *J*-band spectra has already been presented in Das et al. (2006), it is not included here. However, to facilitate studying the overall evolution of the object in the *J*, *H* and *K* bands, we show three representative *J*-band spectra in Fig. 4 and also expanded views of selected *H*- and *K*-band spectra. These spectra in Fig. 4 enable a proper line identification to be made and to also bring out the weaker lines which are not easily discernible in Figs 2 and 3. The line identification is given in Table 3 and certain related aspects are discussed in more details below.

Over the span of our observations, the H I recombination lines remain prominent in the *JHK* spectra – these include Br γ in the *K* band, Br10 to 21 in the *H* band and Pa β and Pa γ in the *J* band. Among the He I lines, those at 1.0830, 1.7002 and 2.0581 μm are prominent. The other weaker lines of He I detected are those at 1.1969, 1.2527, 1.2968, 2.1120 and 2.1132 μm . The other prominent lines in the spectra are the Ly β fluoresced 1.1287 μm and continuum fluoresced 1.3164 μm OI lines, respectively, and two lines at 1.6872 and 1.7414 μm which we attribute to Fe II. A more detailed discussion on these Fe II lines is made in a following subsection. Nitrogen is detected as a broad feature centred around 1.245 μm which is seen conspicuously in the spectrum soon after outburst (top panel of Fig. 4). This feature, which could be a blend of N I lines at 1.2461 and 1.2469 μm , weakens with time but can still be readily discerned in the later spectra (second and third panel from top of Fig. 4) on the blue wing of the He I 1.2527 μm line. An additional N I feature, a blend of the N I 1.2074 and 1.2096 μm lines, also appears to be detected (however see Evans et al. 2007a who attribute this feature to OII 1.2084 μm). Weak features of carbon are also possibly being detected. Immediately after outburst (top panel of Fig. 4), a broad conspicuous bump is seen centred around 1.175 μm . This feature could be a blend of several carbon lines that lie between 1.1653 and 1.1886 μm (the strongest of these are the 1.1748, 1.1753 and 1.1755 μm lines – the blended feature of these lines appears to persist weakly at 1.1748 μm for quite some time after outburst). These carbon lines which are weak here can be extremely strong in novae which have less massive central WDs (CO novae) e.g. in V1280 Sco (Das et al. 2008) and V2274 Cyg (Rudy et al. 2003). In this context it is noted that the analysis of optical and X-ray spectra indicates the ejecta to be enriched in nitrogen and depleted in carbon (Ness et al. 2009 and references therein).

Among the coronal lines, we detect [Si VI] 1.9641 μm , [S IX] 1.2520 μm , [Al IX] 2.0444 μm and a line at ~ 2.09 μm which could possibly be [Mn XIV] 2.0887 μm . The [Si VI] 1.9641 μm line appears at the edge of our instrument spectral window, i.e. in a region of low instrument and atmospheric transmission. The spectrum in this region is noisy making it difficult to accurately estimate the strength of the line. However, we can state, with a fair level of confidence, that the line begins to be clearly detected in the spectrum of 2006 March 26.88. This sets an upper limit on when the line began to be seen in the *K* band. On the other hand, it is difficult to be definitive about when the [S IX] 1.2520 μm line first begins to appear because it is severely blended with the He I 1.2527 μm line. However, from

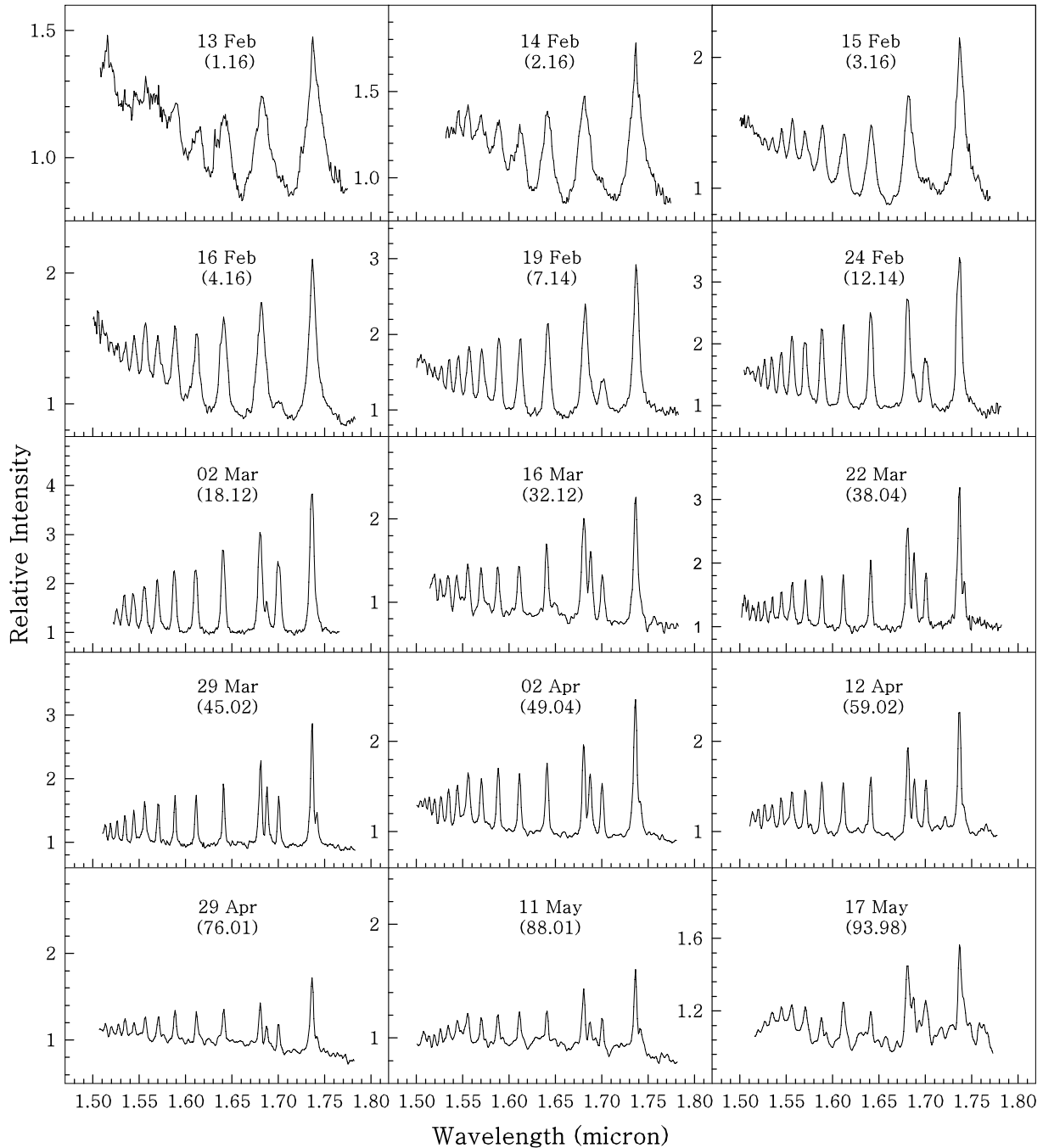


Figure 2. The *H*-band spectra of RS Oph on different days with the flux normalized to unity at 1.65 μm . The number inside the brackets represents the days elapsed since outburst.

an examination of all our *J*-band spectra (Das et al. 2006), we see a significant strengthening of the 1.2527 He I plus [S IX] feature between March 20 and 29. It is likely that this strengthening is due to the emergence of the [S IX] 1.2520 μm line at around this time. Though the identification is uncertain, we attribute the observed line at $\sim 2.09 \mu\text{m}$ to [Mn XIV] 2.0894 μm . The [Mn XIV] 2.0894 μm line is not one among the commonly observed coronal lines in novae. Wagner & Depoy (1996) did observe a line at 2.092 μm in nova V1974 Cyg during its coronal phase and tentatively assigned it to [Mn XIV] 2.0894 μm . An analysis of the temporal evolution of the coronal lines is given in Section 3.7.

There is no evidence for dust formation in the ejecta till the end of our observations. Neither the *JHK* magnitudes show a development of an IR excess nor do the slope of the continua in the spectra shows an upturn towards longer wavelengths indicative of dust formation. It may be noted that *Spitzer* observations obtained over the period 208–430 d after the eruption revealed evidence for silicate dust features at 9.7 and 18 μm (Evans et al. 2007b). However, this silicate dust appears not to have formed in the nova ejecta; rather it has been interpreted as being a part of the red giant wind that existed prior to the 2006 eruption and has survived the outburst (Evans et al. 2007b).

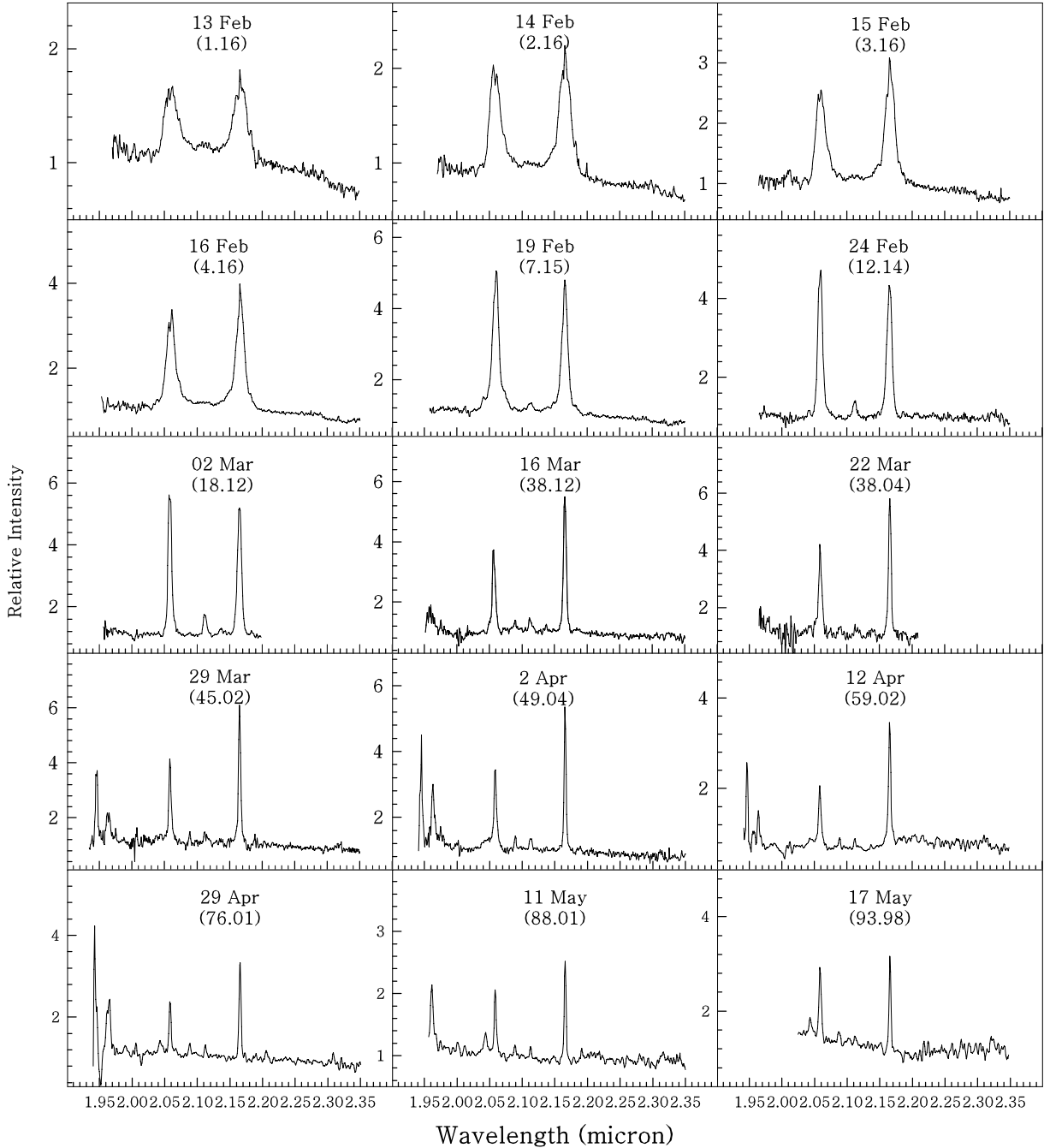


Figure 3. The K-band spectra of RS Oph on different days with the flux normalized to unity at 2.2 μm . The presence of noise and weak features at $\sim 2.0 \mu\text{m}$ in some of the spectra are residuals from incomplete telluric subtraction as discussed in Section 2. The number inside the brackets represents the days elapsed since outburst.

All the emission lines in the H and K bands (Figs 2 and 3) show a rapid narrowing with time similar to what was earlier reported for the Pa β 1.2818 μm and OI 1.1287 μm lines in the J band (Das et al. 2006). Such behaviour was interpreted in terms of the deceleration of the shock wave as it propagated through the pre-existing red giant wind. Since a detailed analysis of the evolution of the shock, from line profile analysis, has already been presented for the J-band lines, we do not repeat a similar analysis for the emission lines seen in the H and K bands. However, we may briefly mention that the Br γ line was similarly analysed as the J-band lines and its line velocity shows a similar temporal evolution as the Pa β line.

3.3 Evidence for a bipolar flow

A significant finding that has emerged from studies of the present outburst of RS Oph is the presence of extended structure in the ejected material. Images from the *Hubble Space Telescope*, taken 155 and 449 d after outburst in the [O III] 5007 \AA and [Ne III] 3426 \AA lines, clearly show an expanding hourglass shaped nebula around RS Oph (Bode et al. 2007; Harman et al. 2009). Such bipolar structure is commonly encountered in planetary nebulae and explained on the basis of the ejecta interacting with a non-uniform circumstellar environment. Alternatively, the ejection of the material could

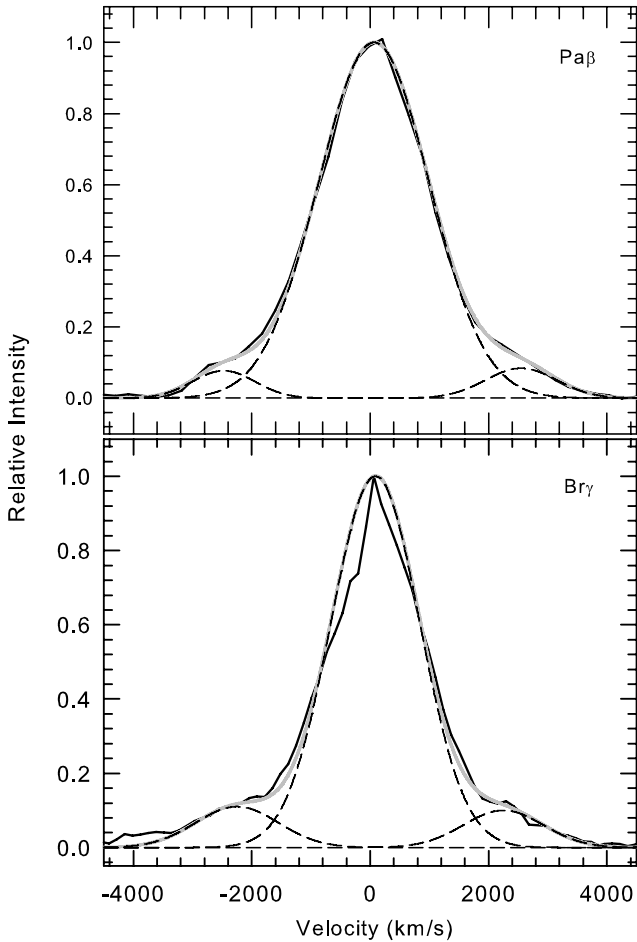


Figure 5. Line profiles of the Pa β and Br γ lines on February 16.987 showing broad wings indicative of a bipolar flow. A multi-Gaussian fit of the profiles is shown – a Gaussian for the central component and two Gaussians for the satellite components in the wings. The Gaussians are shown by dashed lines, their co-added sum by the grey line and the observed data by the continuous black line. Further details are provided in Section 3.3.

by two weaker high-velocity components in the wings (fig. 2 of Skopal et al. 2008).

Similar evidence for a bipolar flow is also seen from our near-IR data. To illustrate this, we present in Fig. 5, representative profiles of the Pa β and Br γ lines on February 16.987. As can be seen, the profiles have a strong central component flanked by two weaker components. In both panels of Fig. 5, we have fitted the profile with three Gaussians – a central Gaussian for the core emission component and two Gaussians for the satellite components in the wings (the Gaussians are shown by dotted lines, their sum by the grey line and the observed data by the continuous black line). It is seen that a three-component Gaussian fits the data reasonably well. The fits indicate the presence of two high-velocity components at radial velocities of -2540 and $+2485$ km s $^{-1}$ for Pa β and at -2340 and 2160 km s $^{-1}$ for the Br γ lines, respectively [these high-velocity components appear to be associated with the faster structure reported by Chesneau et al. (2007)]. The central components have full width at half-maximum (FWHM) of ~ 2200 and 1770 km s $^{-1}$ for the Pa β and Br γ lines, respectively. We can interpret the results of Fig. 5 as follows viz. the core emission can be associated with the slower expanding material from the waist of the bipolar ejecta while the higher velocity satellite components are associated with

the flow from the polar regions. It may be mentioned that Skopal et al. (2008) draw a similar interpretation from their H α profiles.

3.4 The Fe II lines at 1.6872 and 1.7414 μ m

One of the more uncommon spectral features that are seen in our H-band spectra are prominent lines of Fe II at 1.6872 and 1.7414 μ m. In addition, also present in our J-band spectrum of RS Oph is the 1.1126 μ m Fe II line. This line constitutes one of the so-called ‘1 μ m Fe II lines’ that are detected at 0.9997, 1.0171, 1.0490, 1.0501, 1.0863 and 1.1126 μ m in novae (Rudy, Rosano & Puetter 1991; Rudy et al. 2000). The 1 μ m lines, termed so by Rudy et al. (1991) because of their wavelength location, were first identified by Johansson (1977) in the spectrum of η Carinae and later seen in a variety of emission-line stars (Johansson & Jordan 1984; Hamann & Persson 1989; Rudy et al. 1991; Hamann et al. 1994) and in active galactic nuclei (AGN; Rudy et al. 2000, 2001; Rodriguez-Ardila et al. 2002). In comparison, the H-band Fe II lines are rather uncommon, at least in novae spectra. In the case of novae, two of the earlier recorded instances of these lines are in the slow nova V2540 Ophiuchi (Rudy et al. 2002) and possibly also in the recurrent nova CI Aquila (Lynch et al. 2004). One of the main processes for the excitation of the Fe II lines is considered to be Ly α fluorescence. Additional excitation mechanisms are Lyman continuum (Lyc) fluorescence and collisional excitation. Collisional excitation, which can play a significant role in enhancing the strength of the Fe II lines (Bautista, Rudy & Venturini 2004), is discussed in greater details in Section 3.5. We first consider the Ly α fluorescence process for the 1 μ m lines. These lines specifically come from a three step process viz. the line proper comes from the decay of the $3d^5 4s^2 b^4 G$ term at ~ 6.72 eV above the ground state; this term being fed as a second step from decay of a $4G^o$ term at ~ 13.5 eV which is originally pumped in the first step by Ly α fluorescence (Johansson & Jordan 1984).

In this context, we examine the viability of a similar Ly α excitation mechanism for the 1.6872 and 1.7414 μ m lines (it appears that the excitation mechanism for these lines has been studied relatively less compared to the 1 μ m lines). Using the atomic line data base of Kurucz (<http://cfa-www.harvard.edu/amp/ampdata/kurucz23/sekur.html>) we identify, at the relevant wavelengths, two Fe II lines at 1.6872 and 1.7414 μ m which can undergo a similar three-step Ly α excitation process. The 1.7414 μ m line results from the decay of the $3d^6(^3F)4s c^4 F$ term at ~ 6.222 eV above the ground state; the 1.6872 μ m line from the $d^5 4s^2 G$ term at 9.743 eV. It so happens that both these upper levels of the 1.6872 and 1.7414 μ m lines can be fed by not just one, but in fact by several high lying levels – each of these high lying levels capable of being pumped by Ly α photons. As examples for the 1.6872 μ m line we note that photons at 1215.691 and 1215.707 \AA , which are closely coincident with the Ly α line centre at 1215.671 \AA , can excite transitions from low lying levels in Fe II (at around 3.2 to 3.4 eV above ground state) to the higher excited levels (at around 13.4 to 13.6 eV). These higher levels can then decay via ultraviolet (UV) photons (at 1722.607 and 1683.961 \AA , respectively) to the upper level of the 1.6872 μ m transition (viz. the $d^5 4s^2 G$ term). Similarly for the 1.7414 μ m line, photons at 1215.691 and 1215.873 \AA can Ly α fluoresce from low lying levels in Fe II to the higher excited levels. These higher levels can then decay via UV photons (at 3370.341 and 3435.801 \AA , respectively) to the upper level of the 1.7414 μ m transition (viz. the $3d^6(^3F)4s c^4 F$ term). Since H I lines in novae (Ly α included) are routinely broad with widths extending up to a few thousands of km s $^{-1}$, additional Fe II transitions at wavelengths away from the

$\text{Ly}\alpha$ line centre could also contribute to the $\text{Ly}\alpha$ fluorescence process. It is noted from the Kurucz data, that there are indeed quite a few such lines – within a few Angstroms of the $\text{Ly}\alpha$ line centre (1 Å corresponds to about 250 km s^{-1} at the $\text{Ly}\alpha$ wavelength) – that could also contribute to the $\text{Ly}\alpha$ fluorescence process. It thus appears that $\text{Ly}\alpha$ fluorescence is a viable mechanism for the excitation of the 1.6872 and 1.7414 μm lines.

In addition, it also needs to be examined whether $\text{Ly}\alpha$ photons can also play a role in exciting these lines. If the nova ejecta is optically thick in $\text{Ly}\alpha$, as is expected, then it should be optically thick in $\text{Ly}\alpha$ photons too – hence $\text{Ly}\alpha$ fluorescence could also take place. We find that this is indeed viable since several transitions of Fe II can be identified which are excited by $\text{Ly}\alpha$ photons to high-lying energy levels and subsequently followed by decay, via emission of an UV photon, to the upper levels of the 1.6872 and 1.7414 μm lines (one of several examples is the Fe II transition at 914.846 \AA between lower and upper states at 0.083 and 13.636 eV, respectively, which can be the subsequent decay of the higher excited state via a 1672.578 \AA line populates the upper level of the 1.7414 μm line).

Rudy et al. (2002) assigned the observed H -band lines with Fe II lines at 1.6873 and 1.7414 μm . We would agree with the identification of the 1.7414 μm line since a mechanism exists to account for its presence viz. $\text{Ly}\alpha$ and $\text{Ly}\alpha$ fluorescence as has been discussed. However, there is a possibility of an error in the identification of the 1.6873 μm line. It is seen that actually there are two closeby lines of Fe II in this region viz. at 1.68732 and 1.68719 μm , respectively (air wavelengths). Identification of the observed feature with the 1.68719 μm (we refer to this as the 1.6872 μm line throughout the text) appears correct since this line, as demonstrated, can be excited by $\text{Ly}\alpha$ fluorescence. On the other hand the 1.6873 μm line, proposed by Rudy et al. (2002), arises in emission as a transition between the (3F) $4s \text{ } c^4F$ and (5D) $4p \text{ } z^4F$ states at ~ 6.219 and 5.484 eV, respectively. We are unable to identify any transition, arising from $\text{Ly}\alpha$ fluorescence, that can feed the upper level of this line directly or in a secondary step (as in the case of the other observed Fe II lines discussed so far). It therefore appears that the correct identification of the observed feature should be with the 1.68719 μm line.

3.5 Site of the near-IR line emission and studying the possibility of shock breakout

We study whether it is possible to identify the region in the ejecta from where the Fe II and the other near-IR emission lines arise. The excitation mechanism of the Fe II lines could offer a clue in this matter. While $\text{Ly}\alpha$ fluorescence could be a vital or possibly even the central process in exciting the Fe II lines, it may not be the sole mechanism and collisional excitation also plays a significant role. Such an inference is suggested from observations which show the absence, or greatly reduced strength from expected values, of the cascade lines that feed the upper levels of the 1 μm lines (Bautista et al. 2004 for a detailed discussion of the observational evidence). Bautista et al. (2004) show that Fe II has several high-energy pseudo-metastable levels and that collisional coupling between such metastable levels and radiative-emitting levels is considerable. They show that electron-impact-induced transitions from metastable levels strengthens lines throughout the emission spectrum and in particular strengthens the lines that result from secondary decay after $\text{Ly}\alpha$ pumping like the 1 μm lines. Model calculations of the emissivities (Bautista et al. 2004; fig. 1 therein) show that the peak emissivities of lines can be enhanced by a factor of 10 or more when collisional transitions are taken into account vis-à-vis when these transitions

are neglected in the calculations. The emissivities of the lines are found to be dependent strongly on the electron density and peak emissivities are seen to occur at high densities in the range 10^{10} to $10^{12} \text{ electrons cm}^{-3}$. The need for high particle densities to make these lines prominent is not surprising – it is under such conditions that the number of collisional excitations from the metastable levels can be expected to be enhanced. In essence, the model calculations suggest that if the 1.6872, 1.7414 μm lines or the 1 μm lines are strong, then high-density conditions are likely to be prevalent in the ejecta. This in turn, could offer an insight into the site of the Fe II emission. From an inspection of Figs 2 and 3 it is seen that the 1.6872 and 1.7414 μm lines remain prominent throughout the entire span of the observations. Since both lines flank the redward wings of Br11 and Br10 lines, respectively, they are difficult to resolve as separate lines – even if they are present – during the early phases of the expansion when all the emission lines are broad. However, in spite of this, the presence of the 1.6872 μm line can be seen as a discernible inflection on the red wing of Br11 in the February 19 spectrum. We interpret this to mean that high-density conditions prevail from almost the beginning to the end of the observations in 2006 mid-May in spite of the considerable reduction in density that should be expected as the ejecta expands (in case of a geometric dilution with time, i.e. n_e proportional r^{-2} , the electron density is expected to drop by a factor of around 250 to 1000 between February 15–19 and our last observation on May 17).

A possible site, where such high-density conditions can be generated and sustained as long as the shock lasts, is the region of discontinuity that is formed in a shock when a fast wind flows into a slow wind. Recent one-dimensional hydrodynamical models have been developed by Vaytet, O’Brien & Bode (2007) to study the structure and evolution of such a shock in the RS Oph system. Their models aim to revise and improve earlier studies (O’Brien, Bode & Kahn 1992) by taking into account the ejection of material in the outburst as well as allowing the duration of the fast wind phase to be varied, as opposed to the instantaneous release of pure energy employed in their previous Primakoff-type models. In addition, Vaytet et al. (2007) also include the effects of radiative cooling from the shocked gas which can significantly affect the dynamics of the system. Their model calculations show a complex structure for the shock front revealed through the presence of both forward and reverse shocks, with a separating contact discontinuity. In both their updated models viz. the adiabatic wind model and the radiatively cooled model, the contact discontinuity is found to be the site of high-density and low-temperature conditions (relative to the material in the forward and reverse shocked regions). These effects (enhancement of density and lowering of temperature) are more pronounced in the radiatively cooled model.

In view of the above, we thus propose that the Fe II emission, which is apparently favoured by high-density conditions, originates from a region associated with the contact discontinuity. In addition, Fe II is an ion of low ionization stage implying that it should originate in a zone of low kinetic temperature (a similar reasoning applies for the presence of neutral OI lines and suggests it coexists with Fe II). If our premise of associating the Fe II emission with the dense matter at the contact discontinuity is correct, then the fact that prominent Fe II emission is seen even up to ~ 90 d after outburst would imply that the shock front had not broken out even at that stage. When is breakout expected? The answer to this is complicated because of the bipolar velocity flow in the nebula. Since the polar flow is much faster than the equatorial flow (Fig. 5, Section 3.3), it should breakout much earlier. On the other hand, again from Fig. 5, there appears to be much lesser contribution to the line luminosity

from the high-speed bipolar jets vis-à-vis that from the equatorial flow. Thus even if a breakout takes place in the polar direction and contribution to Fe II emission from this region ceases, the bulk of the Fe II emission will still be expected from the shock front in the equatorial plane that has still to break out. In general, breakout will occur when the shock front traverses a distance equal to the finite extent of the red giant wind – this equals the product of the velocity of the red giant wind and the time elapsed since the 1985 outburst (i.e. 21 yr). The velocity of the red giant wind has been estimated to be in the range $10\text{--}20\text{ km s}^{-1}$ (Gorbatski 1972). For this velocity range and adopting a mean value of 1000 km s^{-1} for the shock front velocity in the equatorial plane (from the FWHM values reported in Das et al. 2006), breakout in the equatorial direction could be expected between 75 and 150 d. This time-scale is consistent with our conclusion that breakout may not have occurred till even ~ 90 d after outburst. The breakout time estimates are susceptible to errors because of uncertainties in the parameters involved (viz. the velocities of the red giant wind and the shock front). However, recombination analysis of the H I lines in the following section is reasonably in line with the conclusions drawn here.

3.6 Recombination analysis of the H I lines

We present in Fig. 6 the recombination case B analysis for the H I lines on six reasonably equispaced epochs that sample the evolu-

tion up to 94 d after the outburst. The observed spectra were flux calibrated using the *JHK* magnitudes of Table 2 after correcting for reddening using $E(B - V) = 0.73$ (or $A_v = 2.26$; Snijders 1987). The observed line luminosities were then compared with the case B emissivities of Storey & Hummer (1995). Three points may be made regarding Fig. 6. Since case B calculations are only mildly sensitive to changes in the electron density n_e and temperature T , we have shown by the grey-shaded area, the case B predictions (normalized to unity at Br14) for the parameter space of n_e varying between 10^5 and 10^{12} cm^{-3} and T varying between 5000 and 20 000 K. By showing an extended range in the parameter space, it becomes easier to establish when observed data clearly falls outside the range of plausible model values. The second point concerns the errors involved in comparing the luminosities of lines situated in different bands (Pa β in *J* band, Br10–21 in *H* band and Br γ in *K* band). The robustness of the estimated line luminosities depends on how reliably the flux in the continuum has been calibrated in each of these bands which in turn depends on how reliable is the estimate of the reddening in the band concerned (the amount of extinction in each of the *J*, *H* and *K* bands is different). Thus as a cross-check for the extinction of $A_v = 2.26$ obtained by Snijders (1987), we note that modelling of the galactic interstellar extinction by Marshall et al. (2006) indicates a extinction in the direction of RS Oph of $A_k = 0.21$ to 0.25 (or $A_v = 2.1$ to 2.5 for $A_v = 10 A_k$) for an adopted distance of 1.6 kpc (Snijders 1987) to the source. Thus there is a

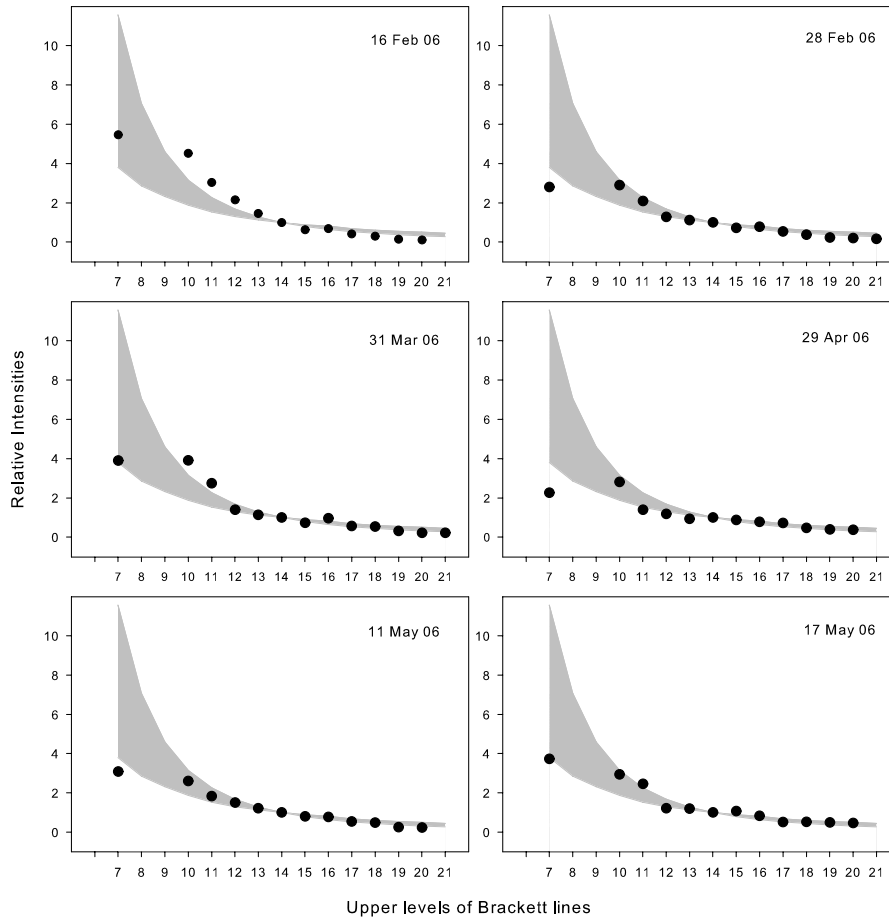


Figure 6. A comparison of the observed Br line intensities on different days with case B predictions. The shaded area in each panel indicates the range over which the case B model values are spread for the electron density n_e varying between 10^5 and 10^{12} cm^{-3} and temperature T between 5000 and 20 000 K. The Br lines have been normalized to unity at Br14, for both case B values and also for the observed data. The error in the strengths of the Br10 and 11 lines is ~ 30 per cent and in the range of 10 to 15 per cent for the other lines. Further details are given in Section 3.6.

consistency in the A_v values estimated by different authors and it is unlikely that major errors are being introduced in the analysis by an incorrect estimate of A_v . The third point concerns the difficulty in estimating the equivalent widths (and hence line luminosities) of the Br10 and 11 lines because they are so strongly blended with the Fe II lines. We have measured the equivalent widths of these lines after trying to deblend the features using Gaussian fits but the exercise is not entirely satisfactory. Thus, while we do show the Br10 and 11 lines in Fig. 6, their strengths are subject to considerable uncertainty (of about 30 per cent) and they should be accepted with caution; the formal error in the strength of the other lines is in the range of 10 to 15 per cent.

Examination of the spread in the case B values in Fig. 6 (the grey-shaded area) indicates that the higher Br lines (Br15 to 20) are really not sensitive enough to discriminate whether there are deviations between the observed data and case B model values. The lines that are sensitive are Br γ and Pa β . In RS Oph, except for the 2006 February 16 data, it is seen that Br γ is consistently weaker than expected and that the Br γ /Br14 ratio is generally in the range of 2–4 against an expected median value of ~ 6 . There is also a suggestion that Br10 and Br11 are stronger than expected and Br10 nearly equal to or stronger than Br γ on all days except February 16. Departures in the ratio of Pa β /Br γ from case B are also seen – this ratio is expected to be around 6 whereas we obtain values of around 6.5, 9.5, 11.5, 15, 11 and 6 for the 6 d shown in Fig. 6. Thus the Pa β /Br γ ratio diverges considerably from case B on most days except February 16 and May 17. However, on May 17, the Br lines do not conform to case B behaviour – the Br γ /Br14 ratio is low. The general conclusion that is therefore suggested, after taking into account the behaviour of all the H I lines, is that the February 16 data conform to a reasonable extent with case B conditions; on other days there are marked deviations from it. On these days, the observed behaviour of the Br lines, i.e. the presence of a Br γ line that is weaker than expected when compared to the higher Br lines accompanied by the additional observation that the Br line strengths are possibly peaking around Br10 to 11 (instead of at Br γ), suggests that the Br lines are optically thick. Such behaviour of the Br lines has been observed in other novae like Nova Ophiuchi 1998 (Lynch et al. 2000) and V4643 Sgr (Ashok et al. 2006) and also in Be stars (Banerjee, Janardhan & Ashok 2001). Such effects have been shown by Lynch et al. (2000) to arise from optical depth effects in an environment with high particle densities ($n_e = 10^{10}$ to 10^{12} cm $^{-3}$) which tends to thermalize the level populations through collisions. It would thus appear that invoking high-density conditions could explain the observed deviations from case B. It is also noted that such high-density conditions prevailed throughout our observations except in the very beginning at around 2006 February 16. At this stage, just 4 d after the outburst, the ejecta has been clearly shown to be in a free expansion stage. That is, it had not yet swept up enough of the red giant wind for the deceleration to begin and possibly for the dense contact surface of the shock front to fully develop. Hence, the high-density conditions, that can create a departure from case B, were likely to be absent at this time. The Fe II line analysis of the previous subsection, which also suggested the need for high-density conditions, is consistent with the line of argument suggested here.

3.7 Evolution of the coronal lines

We consider the temporal evolution of the [Si VI] 1.9641 μm and the [Mn XIV] 2.0894 μm coronal lines here. The uncertainty in the assignment of the latter line to [Mn XIV] has already been discussed in

Table 4. Evolution of the coronal lines.

Date of observation	Days after outburst	Line flux ($\times 10^{-14}$ W m $^{-2}$)	
		[Si VI]	[Mn XIV]
March 2.9465	18.1165	–	0.445 \pm 0.045
March 16.9465	32.1165	–	1.105 \pm 0.195
March 18.9372	34.1072	–	0.790 \pm 0.110
March 19.8833	35.0533	–	0.730 \pm 0.100
March 22.8682	38.0382	–	0.635 \pm 0.115
March 26.8778	42.0478	1.350 \pm 0.160	0.450 \pm 0.040
March 27.8644	43.0344	2.235 \pm 0.065	0.365 \pm 0.045
March 29.8462	45.0162	2.540 \pm 0.240	0.430 \pm 0.070
March 30.8629	46.0329	3.500 \pm 0.320	0.435 \pm 0.125
March 31.8701	47.0401	3.070 \pm 0.430	0.265 \pm 0.025
April 2.8736	49.0436	2.615 \pm 0.255	0.345 \pm 0.065
April 3.9691	50.1391	2.430 \pm 0.280	0.355 \pm 0.035
April 5.9607	52.1307	2.270 \pm 0.110	0.340 \pm 0.030
April 12.8454	59.0154	1.560 \pm 0.090	0.300 \pm 0.070
April 22.9392	69.1092	1.475 \pm 0.275	0.360 \pm 0.100
April 29.8355	76.0055	1.360 \pm 0.050	0.255 \pm 0.065
May 3.8100	79.9800	1.235 \pm 0.165	0.225 \pm 0.085
May 11.8353	88.0053	0.785 \pm 0.075	0.118 \pm 0.043
May 17.8103	93.9803	0.705 \pm 0.135	0.117 \pm 0.023

Section 3.2; we proceed by assuming that this assignment is correct. The observed strength of these lines on different days is presented in Table 4 and their temporal evolution is shown in Fig. 7. The [Si VI] line is first detected clearly on around March 26.88 (~ 42 d after outburst). It then increases in strength, peaking at around March 30.86 (~ 46 d after outburst) and subsequently declines in intensity. The [Mn XIV] line appears on March 2.95 (~ 18 d after outburst), earlier than the [Si VI] line, but shows a similar evolution in the sense that it increases in strength with time and subsequently declines. Unfortunately, no spectra were recorded between 2006 March 3 and 16 (i.e. 18 to 32 d after outburst) to monitor the evolution of the [Mn XIV] line during this period. The observed temporal behaviour of the coronal lines can be interpreted in a simple manner. The coronal lines are expected to arise from the hot, shocked gas in the shock front. This gas, whose temperature in the very early stages was determined to be as high as $\sim 10^8$ K (Sokoloski et al. 2006), gradually cools with time. The fractional abundance of an ion [e.g. N(Si VI)/N(Si)] in a collisionally ionized, low-density plasma is known to be temperature dependent. Model calculations show that the fractional abundance of Si VI peaks at a temperature of 4×10^5 K (Jordan 1969; Shull & van Steenberg 1982) while the Mn XIV ion peaks at 1.6×10^6 K, respectively (Landini & Monsignor Fossi 1972). Since the strength of a line associated with an ion is proportional to the abundance of the ion, it is expected that the strength of the line will change as the temperature of the plasma changes (thereby changing the abundance of the ion). It would appear that this phenomenon is being manifested here. As the shocked gas in the RS Oph system cools, a temperature will be reached that is conducive for the formation of a particular ion to begin. Subsequent lowering of the temperature should see the fractional abundance of the ion reach its peak value at the optimum temperature for its production and the fractional abundance should subsequently decline as the temperature continues to decrease.

The temporal evolution of the [Si VI] and [Mn XIV] lines, as shown in Fig. 7, is consistent with such a scenario (there is, however, a possible complication which is discussed shortly). Further, since the 2.0894 μm line is detected earlier than the [Si VI] line (therefore at a phase when the shocked gas is relatively hotter), the

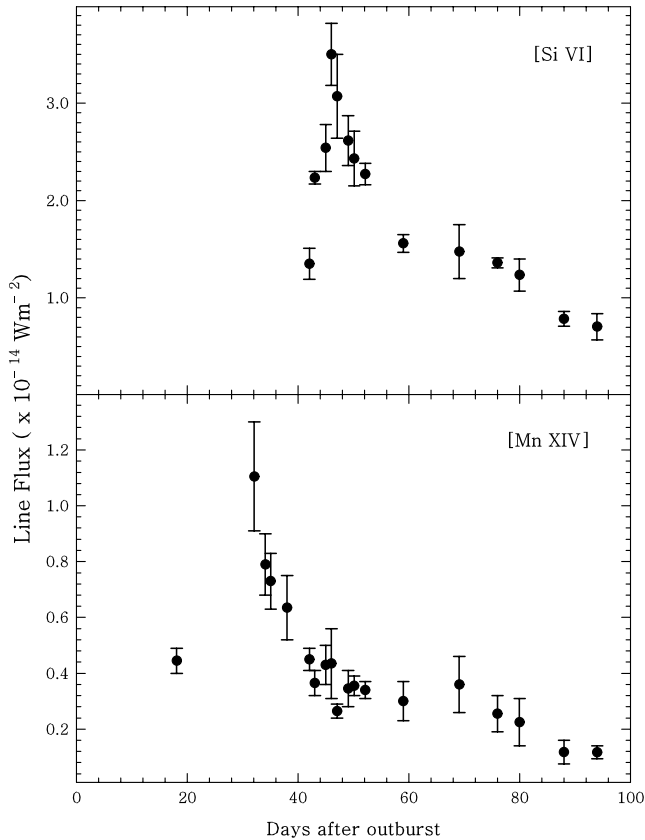


Figure 7. Temporal evolution of the dereddened line strengths of the [Si vi] 1.9641 μm and [Mn xiv] 2.0894 μm lines. Further details are given in Section 3.7.

analysis suggests that it is likely that the 2.0894 μm line originates from an ion with higher ionization potential than Si vi. In this sense it is consistent to identify this line with [Mn xiv] since it has a higher ionization potential of 344 eV compared to 166.8 eV for [Si vi]. Since the [Mn xiv] and [Si vi] line emission peaks on March 16.95 and March 30.86, respectively, the temperatures on these days are indicated to be 1.6×10^6 and 4×10^5 K, respectively, based on the ionization balance models discussed earlier (Jordan 1969; Landini & Monsignori Fossi 1972; Shull & van Steenberg 1982). These temperatures may be compared with those derived from X-ray observations on nearby dates. Nelson et al. (2008) obtain a value of 6.3×10^6 K on 2006 March 11–12 (day 27.7 after outburst; table 4 of Nelson et al. 2008). This is reasonably in agreement with the temperature of 1.6×10^6 K that we obtain on March 16.95. Ness et al. (2007) determine a temperature range of $(6.3\text{--}8.3) \times 10^5$ K on day 39.7 after outburst (2006 March 24) while we get a value of 4×10^5 K on March 30.86. Here too, the temperature estimates are in reasonable agreement with each other.

In the case of RS Oph, a complication that arises in applying models for the fractional ion abundance, based on purely collisional effects, is that the effect of any radiation field is assumed to be negligible. X-ray spectra in the initial stages after outburst clearly indicate that the plasma in RS Oph is collisionally dominated (Nelson et al. 2008). However, these authors observe a supersoft X-ray phase in RS Oph during weeks 6–10 arising from the hot central WD whose temperature was estimated to be 800 000 K. The radiation field from the central WD could thus be expected to affect the ionization balance in the ejecta. We consider it a difficult prob-

lem, beyond the scope of this work, to assess the extent to which the WD radiation field – in conjunction with collisional ionization – affects the ionization balance. We, however, note that our analysis/discussion on the [Mn xiv] line is unlikely to be affected by the supersoft X-ray phase since this phase began towards the end of March (Nelson et al. 2008) after the [Mn xiv] line had peaked in intensity. However, the [Si vi] line emission, could be affected to some extent by the supersoft X-ray phase.

4 SUMMARY

H- and K-band photometry and spectroscopy of the 2006 outburst of RS Oph are presented. This work, in conjunction with the J-band observations presented earlier in Das et al. (2006), documents the near-IR evolution of RS Oph in a detailed manner. An extensive set of spectra has been presented and an analysis and discussion has been made of the emission lines seen therein (H β Pa and Br recombination lines, coronal lines, Fe II lines etc). The Fe II lines at 1.6872 and 1.7414 μm , rather uncommon in novae, have been studied in some details. They appear to arise from a combination of Ly α plus Lyc fluorescence and collisional excitation. The site of origin of the near-IR line emission is explored based on the analysis of the Fe II lines and case B recombination studies. An analysis is made of the temporal evolution of the [Si vi] 1.9641 μm coronal line and another coronal line at 2.0894 μm which is attributed to [Mn xiv]. Assuming collisional effects to dominate in the hot coronal gas, we estimate the coronal temperature to be 1.6×10^6 and 4×10^5 K on 2006 March 16.95 and 30.86, respectively.

ACKNOWLEDGMENTS

The research work at Physical Research Laboratory is funded by the Department of Space, Government of India. We are thankful for the online availability of the Kurucz atomic linelist data base which was extensively used in this work. We thank the referee, Prof. Aneurin Evans, for his suggestions which greatly helped in improving the results presented here.

REFERENCES

- Ashok N. M., Banerjee D. P. K., Varricatt W. P., Kamath U. S., 2006, MNRAS, 368, 592
 Banerjee D. P. K., Janardhan P., Ashok N. M., 2001, A&A, 380, L13
 Bautista M. A., Rudy R. J., Venturini C. C., 2004, ApJ, 604, L129
 Bode M. F. et al., 2006, ApJ, 652, 629
 Bode M. F., Harman D. J., O'Brien T. J., Bond H. E., Starrfield S., Darnley M. J., Evans A., Eyres S. P. S., 2007, ApJ, 665, L63
 Brandi E., Quiroga C., Mikolajewska J., Ferrer O. E., Garca L. G., 2009, A&A, 497, 815
 Buil C., 2006, Cent. Bur. Electron. Telegr., 403
 Chesneau O. et al., 2007, A&A, 464, 119
 Das R. K., Banerjee D. P. K., Ashok N. M., 2006, ApJ, 653, L141
 Das R. K., Banerjee D. P. K., Ashok N. M., Chesneau O., 2008, MNRAS, 391, 1874
 Evans A., Callus C. M., Albinson J. S., Whitelock P. A., Glass I. S., Carter B., Roberts G., 1988, MNRAS, 234, 755
 Evans A. et al., 2007a, MNRAS, 374, L1
 Evans A. et al., 2007b, ApJ, 671, L157
 Fekel F. C., Joyce R. R., Hinkle K. H., Skrutskie M. F., 2000, AJ, 119, 1375
 Fujii M., 2006, IAU, 8869
 Gorbatski V. G., 1972, SvA, 16, 32
 Hamann F., Persson S. E., 1989, ApJS, 71, 931
 Hamann F., Simon M., Carr J. S., Prato L., 1994, ApJ, 436, 292

- Harman D. J. et al., 2009, in Evans A., Bode M. F., O'Brien T. J., Darnley M. J., eds, ASP Conf. Ser. Vol. 401, RS Ophiuchi (2006) and the Recurrent Nova Phenomenon. Astron. Soc. Pac., San Francisco, p. 246
- Hirosawa K., 2006, IAU, 8671
- Iijima T., 2006, IAU, 8675
- Johansson S., 1977, MNRAS, 178, 17
- Johansson S., Jordan C., 1984, MNRAS, 210, 239
- Jordan C., 1969, MNRAS, 142, 501
- Kantharia N. G., Anupama G. C., Prabhu T. P., Ramya S., Bode M. F., Eyres S. P. S., O'Brien T. J., 2007, ApJ, 667, L171
- Landini M., Monsignor Fossi B. C., 1972, A&AS, 7, 291
- Lynch D. K., Rudy R. J., Mazuk S., Puetter R. C., 2000, ApJ, 541, 791
- Lynch D. K., Wilson J. C., Rudy R. J., Venturini C., Mazuk S., Miller N. A., Puetter R. C., 2004, AJ, 127, 1089
- Marshall D. J., Robin A. C., Reyle C., Schultheis M., Picaud S., 2006, A&A, 453, 635
- Monnier J. D. et al., 2006, ApJ, 647, L127
- Nelson T., Orio M., Cassinelli J. P., Still M., Leibowitz E., Mucciarelli P., 2008, ApJ, 673, 1067
- Ness J. U. et al., 2007, ApJ, 665, 1334
- Ness J. U. et al., 2009, AJ, 137, 3414
- O'Brien T. J., Bode M. F., Kahn F. D., 1992, MNRAS, 255, 683
- O'Brien T. J. et al., 2006, Nat, 442, 279
- Rodriguez-Ardila A., Viegas S. S., Pastoriza M. G., Prato L., 2002, ApJ, 565, 140
- Rosino L., Iijima T., 1987, in Bode M. F., ed., RS Ophiuchi (1985) and the Recurrent Nova Phenomenon. VNU Science Press, Utrecht, p. 27
- Rudy R. J., Rosano G. S., Puetter R. C., 1991, ApJ, 383, 344
- Rudy R. J., Puetter R. C., Mazuk S., Hamann F., 2000, ApJ, 539, 166
- Rudy R. J., Lynch D. K., Mazuk S., Venturini C. C., Puetter R. C., 2001, PASP, 113, 916
- Rudy R. J., Lynch D. K., Mazuk S., Venturini C. C., Puetter R. C., Perry R. B., 2002, BAAS, 34, 1162
- Rudy R. J., Dimpfl W. L., Lynch D. K., Mazuk S., Venturini C. C., Wilson J. C., Puetter R. C., Perry R. B., 2003, ApJ, 596, 1229
- Rupen M. P., Mioduszewski A. J., Sokoloski J. L., 2008, ApJ, 688, 559
- Shull J. M., van Steenberg M., 1982, ApJS, 48, 95
- Skopal A., Pribulla T., Buil C., Vittone A., Errico L., 2009, in 'RS Ophiuchi (2006) and the Recurrent Nova Phenomenon'. ASP Conf. Ser. Vol. 401. Astron. Soc. Pac., San Francisco, p. 227
- Snijders T., 1987, in Bode M. F., ed., RS Ophiuchi (1985) and the Recurrent Nova Phenomenon. VNU Science Press, Utrecht, p. 27
- Sokoloski J. L., Luna G. J. M., Mukai K., Kenyon S. J., 2006, Nat, 442, 276
- Storey P. J., Hummer D. G., 1995, MNRAS, 292, 41
- Vaytet N. M. H., O'Brien T. J., Bode M. F., 2007, ApJ, 665, 654
- Wagner R. M., Depoy D. L., 1996, ApJ, 467, 860
- Whitelock P. A., Carter B. S., Feast M. W., Glass I. S., Laney D., Menzies J. W., Walsh J., Williams P. M., 1984, MNRAS, 211, 421
- Worters H. L., Eyres S. P. S., Bromage G. E., Osborne J. P., 2007, MNRAS, 379, 1557

This paper has been typeset from a $\text{\TeX}/\text{\LaTeX}$ file prepared by the author.